Available online at www.sciencedirect.com
ScienceDirect
Journal of the European Ceramic Society 27 (2007) 2045–2052
www.elsevier.com/locate/jeurceramsoc

Dielectric properties of M-type barium hexaferrite prepared by co-precipitation

Kajal K. Mallick *, Philip Shepherd, Roger J. Green

School of Engineering, University of Warwick, Coventry CV4 7AL, United Kingdom

Received 16 February 2006; received in revised form 16 May 2006; accepted 20 May 2006
Available online 4 August 2006

Abstract

Highly stoichiometric and phase pure barium hexaferrite has been synthesized by co-precipitation as well as a solid-state preparative method using high purity nitrates, oxides and carbonates of iron(III), barium(II) and ammonium hydroxide. The isochronal and isothermally measured complex permittivity and dielectric loss tangents over 1 MHz–1 GHz in frequency remained relatively stable until a sintering temperature between 1100 and 1300 °C. A high value of relative permittivity of 32 and low loss tangent of 0.0329 indicate suitable high frequency characteristics for barium hexaferrite. The measured apparent densities before and after each firing cycle showed a monotonic increase. The crystal structure determined from X-ray diffraction studies confirmed the presence of single phase belonging to the theoretical space group *P*63/*mmc* with calculated cell parameters of $a = b = 5.895$ Å and $c = 23.199$ Å. In addition the DTA hexaferrite formation temperature was found to be 1050 °C.

Keywords: Electron microscopy; Dielectric properties; Electrical properties; Ferrites; $BaFe_{12}O_{19}$

1. Introduction

Hexagonal barium hexaferrite ($BaFe_{12}O_{19}$), often denoted as M-type BaM, is widely used for various important electronic applications such as permanent magnets, particulate media for magnetic recording and microwave devices.[1–3] Ferrites and garnets are ferromagnetic oxides with dielectric and magnetic properties that are useful for rf and microwave applications. The high electrical resistivity of ferrites coupled with their low magnetic losses is critical in maintaining low insertion loss in microwave devices. The latter includes multilayer chip inductors as the main surface mount devices (SMDs) usually operated in 0.3–1 GHz frequency range.[4,5] The preparation techniques as well as the structural doping of Co and Ti ions influence the magnetodielectric properties of this compound. For example, Mosallaies[6] used barium hexaferrite mixed with cobalt oxide (Co_3O_4) and barium carbonate ($BaCO_3$), developed at Trans-Tech Inc., and obtained a material with relative permittivity (ε_r) and relative permeability (μ_r) both approximately 16, a loss tangent of 0.001 dielectric and 0.03 magnetic at frequency of 500 MHz. These authors used the material in electronic band-gap (EBG) structures and microstrip patch antenna applications. However, they provided little experimental information as to the material preparation or synthesis method. It is also unclear about the actual stoichiometric composition of their material that has been characterised. Similarly, there are many other conflicting reports of the dielectric properties of BaM with little or scarce information on the ceramic or sol gel preparative methods.[7,8] In the present paper, the co-precipitation route has been used since it is a more reliable method where the stoichiometry can easily be controlled. It is also the aim to characterise fully the physical and dielectric properties of barium hexaferrite as synthesized by an additional solid-state ceramic technique. The paper reports the preparation methods to produce stoichiometric BaM and the associated electrical properties as a function of temperature (isothermal), time (isochronal) and frequency. The electrical property measurements relate to the dielectric loss tangent, relative complex permittivity over a frequency range of 1 MHz–1 GHz as well as the density variation with sintering conditions of the BaM material. Establishing the electrical (permittivity) and loss characteristics (frequency by implication) of the material is necessary in order to design devices for appropriate applications. Furthermore, the phase development and crystal structure are discussed. Magnetic property mea-

* Corresponding author. Tel.: +44 24 7652 2342; fax: +44 24 7652 4027.
E-mail address: k.k.mallick@warwick.ac.uk (K.K. Mallick).

0955-2219/$ – see front matter © 2006 Elsevier Ltd. All rights reserved.
doi:10.1016/j.jeurceramsoc.2006.05.098

surements are still in progress and will be reported at a later date.

2. Experimental

2.1. Synthesis

Stoichiometric composition of BaM was synthesized using a chemically reliable co-precipitation route as well as the well-known solid-state synthesis method from relevant oxides.

The solution route involved a slow and drop wise addition of excess ammonium hydroxide (pH 12) to the aqueous solution consisting stoichiometric amounts of nitrates of Ba and Fe (99.99% purity, Aldrich) that resulted in the co-precipitation of a gel like cake. The cake was thoroughly washed with deionised water and purified ethanol, dried at 105 °C and was subsequently heated to various temperatures.

The ceramic method involved firstly the formation of stoichiometric monoferrite, $BaFe_2O_4$ using $BaCO_3$ (99.999% purity, Aldrich) and Fe_2O_3 (99.98% purity, Aldrich) as raw constituents, followed by further reaction with excess Fe_2O_3 to obtain barium hexaferrite. Following intermittent heating at 800 °C for 3 h and grinding (in an agate pestle and mortar), the final material was pelletised using a Specac uniaxal press to 6000 psi producing disk samples of 16 mm in diameter. Sintering of these pellets was carried out at temperatures ranging from 800 to 1300 °C, the latter being the final sintering temperature. The BaM hexaferrite composition produced by both methods was subjected to identical temperature regimes and time intervals.

2.2. Density measurements

The density of the samples from the green to their sintered state was measured using the well-known Archimedes method. The measurements were carried out to record the change following various sintering treatment protocol.

2.3. X-ray diffraction measurements

X-ray powder diffraction (XRD) patterns for samples treated at various temperatures and times were recorded in the region of $2\theta = 10$–80 °C with a step scan of 0.02 °C/min on a Philips diffractometer (Model PW1710) using Cu Kα radiation. The evolving phases were matched using an automated powder diffraction software package that included both standard ICDD and calculated ICSD diffraction files. Cell parameters were calculated and further refined using linear regression procedures (Philips APD 1700 software) applied to the measured peak positions of all major reflections up to $2\theta = 90$ °C.

The crystallite size was determined using the well-known Scherrer formula,[9] from the line broadening of diffraction profile of the strongest peak. The formula, excluding the effects of the machine broadening to minimize errors, is given below

$$D = \frac{k\lambda}{h_{1/2}} \cos\theta \tag{1}$$

where D is the average size of the crystallites, k the Scherrer constant, λ the wavelength of radiation, $h_{1/2}$ the peak width at half height and θ corresponds to the peak position. The measured values were corrected for the effects due to instrumental broadening.

2.4. Scanning electron microscopy

For the scanning electron microscopy (SEM), a Philips Cambridge Stereoscan was used to determine the morphology of the barium hexaferrite particles as well as to observe related microstructural features of the ferrite particulates.

2.5. Dielectric measurements

The high frequency dielectric properties were measured using an Impedance/Material Analyzer E4991A with a 16453A test fixture for dielectric material measurements, from Agilent Technologies. The frequency of interest was 1 MHz–1 GHz and measured at ambient temperature (25 °C).

The test fixture uses the parallel plate method of determining the permittivity and loss tangent of the material, as shown schematically in Fig. 1(a) and (b). This involves placing the sample material in between two circular plates to form a parallel plate capacitor; an LCR meter then measures the load. The real part of the permittivity (ε') is calculated from the capacitance and the complex part of the permittivity (ε'') is calculated from the measurement of the dissipation factor D.

The capacitor above in Fig. 1(a) has a small capacity due to its large impedance and therefore should be considered as in Fig. 1(b). In this case, the admittance of is equal to

$$Y = G + \mathrm{j}\omega C \tag{2}$$

$$Y = \mathrm{j}\omega\left(\frac{C}{C_\mathrm{o}} - \mathrm{j}\frac{G}{\omega C_\mathrm{o}}\right) C_\mathrm{o} \tag{3}$$

where C and C_o are the capacitance across the plates when the plates are filled with material and air, respectively. Therefore complex relative permittivity is defined as

$$\varepsilon^* = \varepsilon'_\mathrm{r} - \mathrm{j}\varepsilon''_\mathrm{r} \tag{4}$$

and calculated via

$$\varepsilon'_\mathrm{r} = \frac{C}{C_\mathrm{o}} = \frac{tC}{\varepsilon_\mathrm{o} A} \tag{5}$$

$$\varepsilon''_\mathrm{r} = \frac{G}{\omega C_\mathrm{o}} = \frac{t}{\omega \varepsilon_\mathrm{o} A R_\mathrm{p}} \tag{6}$$

where $G \to 1/R_\mathrm{p}$, t the sample thickness and A is the plate area.

Performing a calibration procedure on the test fixture using an OPEN and a SHORT reduces the errors in the system and a known LOAD state before the DUT is measured.[10]

2.6. Thermogravimetric and differential thermal analysis

Thermogravimetry (TG) and differential thermal analysis (DTA) were performed on samples of unsintered green material. A Perkin-Elmer Pyris Diamond TG/DTA was used, over

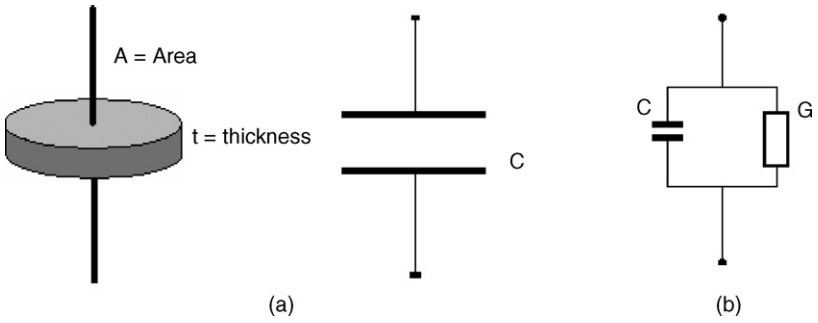

Fig. 1. (a) Parallel plate test fixture measurement method. (b) Equivalent circuit model.

the temperature range of 20–1100 °C, at a rate of 20 °C/min, in static air with platinum crucibles.

3. Results and discussion

3.1. Thermogravimetric and differential thermal analysis

The TG/DTA plots for the as synthesized cake are shown in Fig. 2(a). It can be seen that the endotherm at around 100 °C corresponds to the removal of hydroxyl species present during preparation. The organic species is burnt off at 250 °C indicated by a small exotherm. Thereafter, the weight loss is incremental and an overall loss of about 60% is indicated. The loss is also concomitant with the appearance of an endotherm in the DTA curve at 807 °C. The peak is attributed to the decarboxilation of $BaCO_3$, reported to take place at 1055 °C for pure carbonate,[11] and around 800 °C for the mixture of carbonate and iron oxide.[12] The completion of formation of the hexaferrite is indicated at around 1050 °C. It is to be noted here that the conversion is very rapid and is highlighted by the appearance of a sharp spike associated with the endotherm. The rapid exothermic response at the start of the trace may also be due to the buoyancy effect in the equipment.

Fig. 2(b) shows the traditional, chemically reliable, co-precipitation route TG/DTA plot. It can be seen that the nitrates are fully burned off by 640 °C whereupon the BaM compound is fully formed.

3.2. Crystal structure and particle morphology

The typical XRD patterns of the sintered $BaFe_{12}O_{19}$ hexaferrite compound from the co-precipitation and solid-state ceramic method together with the standard are shown in Fig. 3(a)–(c), respectively.

In the gel stage (cake) following co-precipitation, the structure was found to be partially crystalline and the amount of the residual uncrystallised phase is mainly of amorphous nature characterised by a broadening of the observed peaks. The amorphous nature persisted until 600 °C and became fully crystalline at 1300 °C. When sintered to the final temperature of 1300 °C, a single phase structure is formed prior to and/or during heating cycles. For either the co-precipitation or the solid-state method there is a complete absence of any unreacted residual phases. However, the diffraction patterns for co-precipitated powders were poorly crystallised compared to those obtained by the ceramic method for any given sintering temperature. This is to be expected since the precursor constituents used for ceramic methods are already crystalline and the formation of the compound is merely driven by the thermodynamic criteria. The monophasic patterns obtained by these methods match

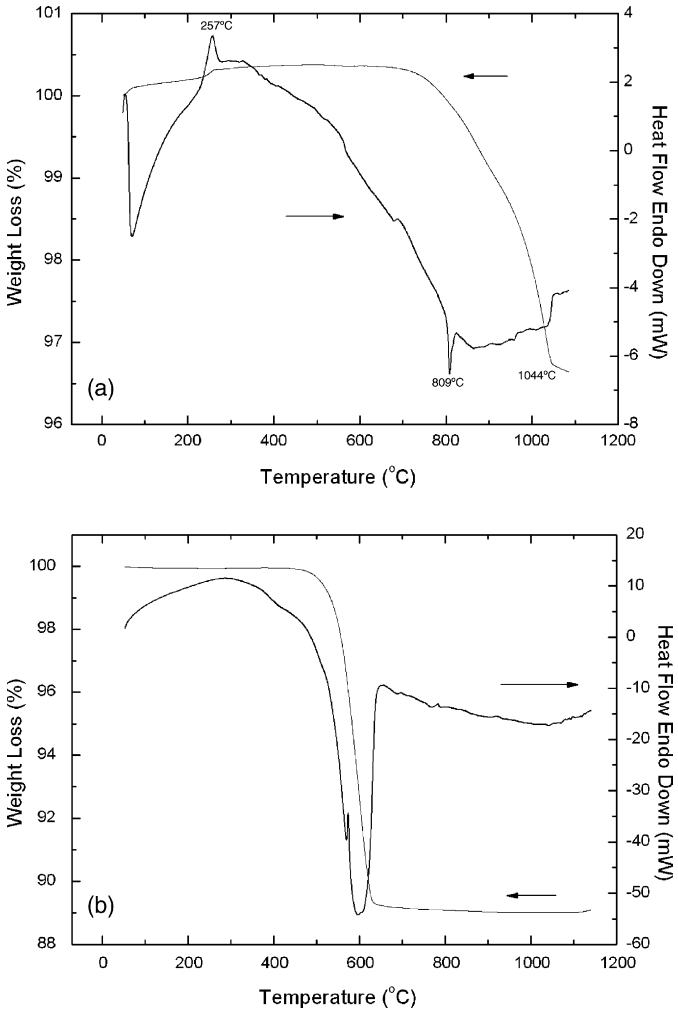

Fig. 2. Thermogravimetry (TGA) and differential thermal analysis (DTA) of the (a) as synthesized co-precipitated cake and (b) solid-state ceramic method compounds.

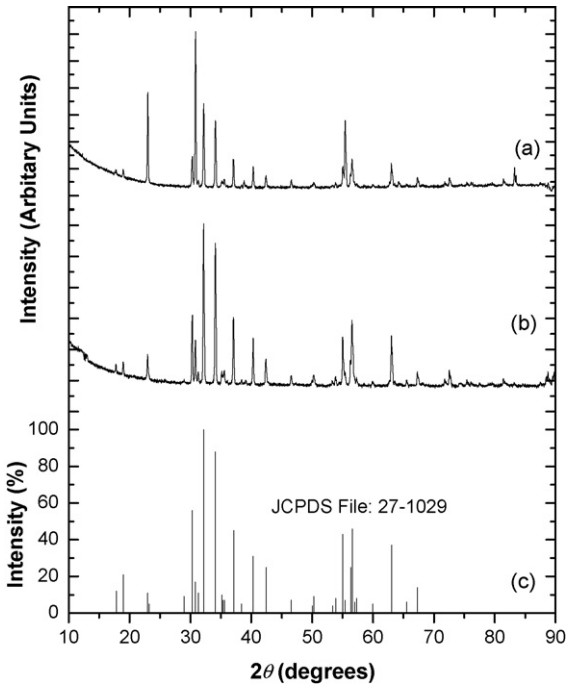

Fig. 3. X-ray diffraction patterns of sample (a) co-precipitation method compound sintered at 1300 °C/1 h; (b) solid-state ceramic method compound sintered at 1300 °C/1 h; (c) standard JCPDS File (27-1029).

exactly the reference standard, JCPDS file no. 27-1029,[13] and this is shown in Fig. 3(c). However, the iron in the material causes a high level of background because it fluoresces, the Cu Kα radiation is very close to Fe energy state. The intensity of the peaks differ from those described in the reference standard and this is due to the preferred orientation of the hexagonal plates found in the material structure. The two unindexed peaks are in the region, $2\theta = 35.365$ (7% intensity) and $2\theta = 71.526$ (1% intensity). These peaks were, as a combination of high background and preferred orientation, not visible. The peaks were indexed as a primitive hexagonal cell with space group, *P*63/*mmc* (194) with the refined lattice parameter values of $a = b = 5.895$ Å and $c = 23.199$ Å. These values agree well with the published literature data.[14–16] The structural representation for this compound is shown in Fig. 4, where the crystal consists of 64 ions per unit cell on 11 different symmetry sites and crystallizes in *P*63/*mmc* space group. The 24 Fe^{3+} atoms are distributed over five symmetry sites, 3 octahedral sites, 1 tetrahedral site and 1 bipyramidal site.

The average crystallite size, determined from the position of the strongest (107) diffraction peak, was found to be in the region of 80–100 nm and 1–2 μm for the co-precipitated gel and sintered samples, respectively. With increasing heat treatment temperatures from 800 to 1300 °C the relative intensity of the 100% peak increased whilst the other peaks becoming equally sharper indicating an increase in particle size.

Figs. 5(a)–(c) shows the morphology of these particles as synthesized as well as the development of grain structure when sintered at 1300 °C. The particles following co-precipitation were found to be composed of two different particle shape and sizes, where the majority are of acicular/platelet form and the

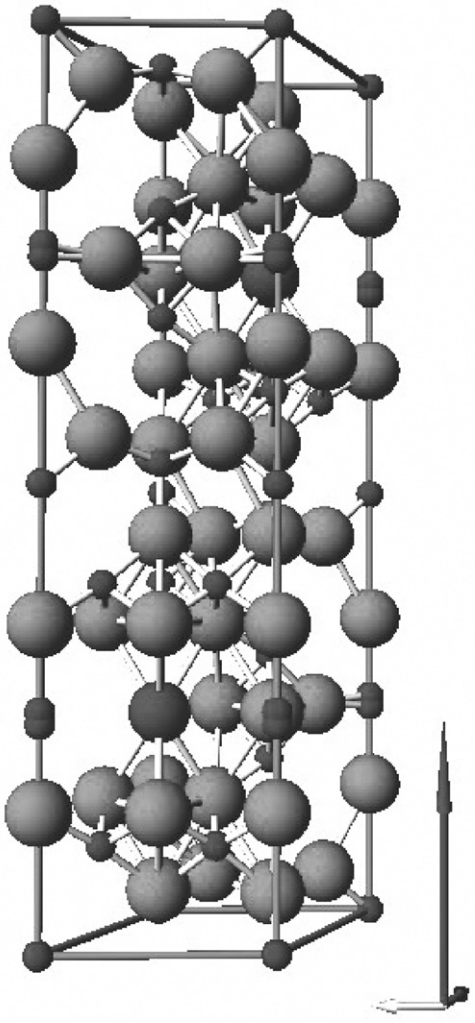

Fig. 4. Structural representation of $BaFe_{12}O_{19}$ (BaM) compound (small filled, light and dark circles = Fe, O and Ba, respectively).

size ranged from 0.5 to 2 μm (Fig. 5(a)). In case for the polished and etched samples sintered at 1300 °C, it is clear, from Figs. 5(b) and (c), that the particles are hexagonal platelet crystals and the average grain ranged from 3.5 to 10 μm with the largest grains in the range of 20–25 μm. There is clear evidence that some of these grains have coalesced to form larger grains within the material formed at high temperature as a consequence of thermodynamically driven mass diffusion mechanisms. An example is shown in Fig. 5(b), where the particles labelled 'A' are of the order of 25 μm wide by 60 μm long. However, these types are less prevalent throughout the material than those uniformly distributed, the grain size of which lies in the region of approximately 5 μm in diameter. It is to be noted here that there are some pores present; in the final structure that is unavoidable since 100% theoretical density is never achieved during any sintering process.

3.3. Variation of density

Fig. 6 shows the isothermal and isochronal variation of density for a typical BaM ceramic over temperatures and time

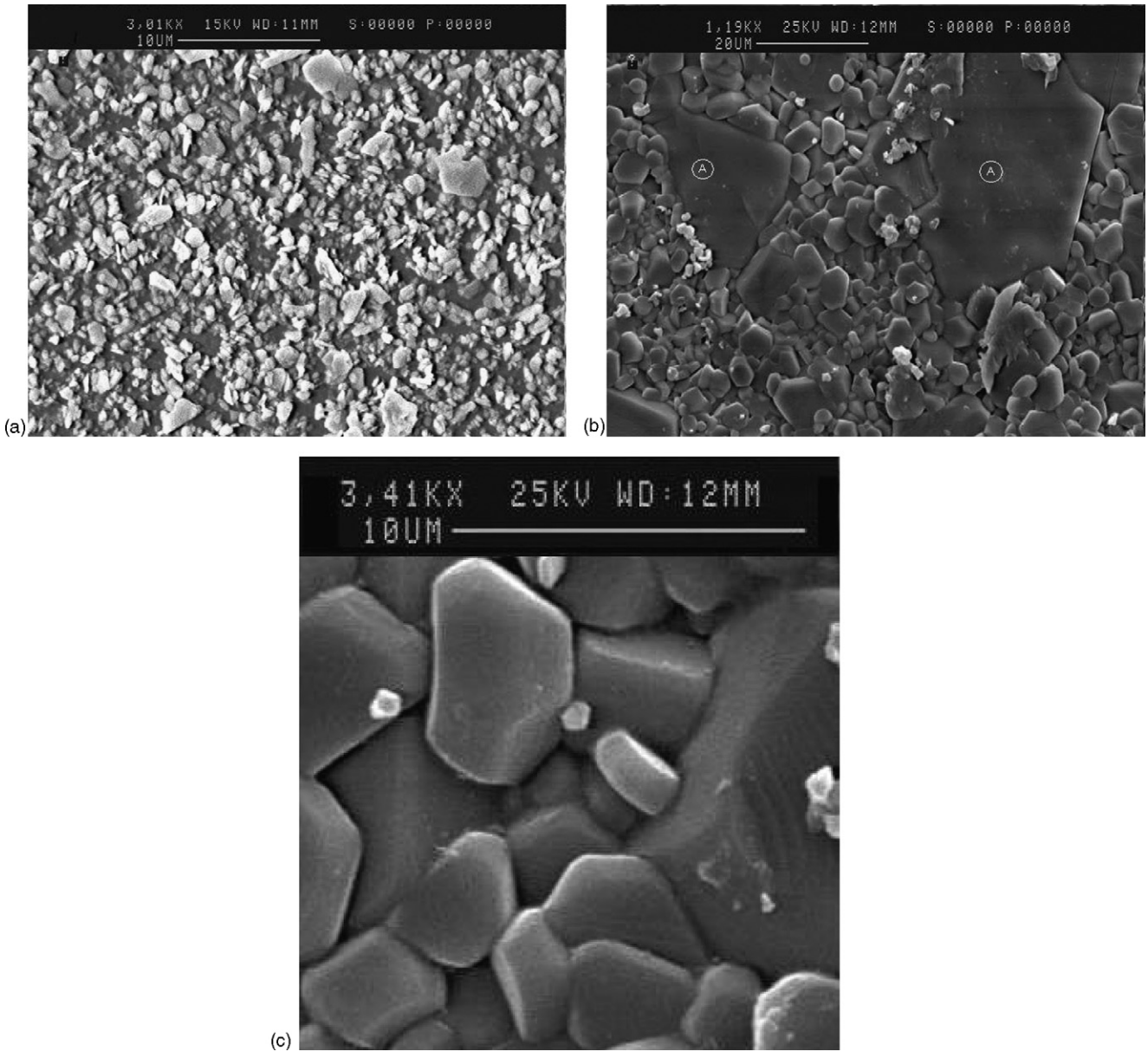

Fig. 5. (a) Morphology of as synthesized co-precipitated particles. (b) Morphology of BaM particles at 1300 °C. (c) Enlarged view of the smaller particles sintered at 1300 °C.

intervals shown. It can be seen that initially the density remained relatively unchanged as the temperature was increased from room temperature to 1100 °C during a treatment time for approximately 50 h. This is expected since no additional binder was employed to consolidate the green product even at this relatively high temperature. However, thereafter the density values increased sharply and monotonically with time, in the temperature window of ca. 1100–1300 °C. For example, a value of final density of 4.9 g/cm^3 was achieved after sintering at 1300 °C for only 1 h. This value compares favourably with the theoretical density of 5.30 g/cm^3 for this material. Hence the density achieved using the co-precipitation route was found to be ∼92.5% of the theoretical density and is quite significant that such a high level of density can be achieved without any sintering aid.

3.4. High frequency dielectric properties

The dielectric properties of the $BaFe_{12}O_{19}$ hexaferrite prepared by co-precipitation are shown in Figs. 7–9. All the measured data refers to a frequency range of 1 MHz–1 GHz at the ambient temperature. These plots refer to the theoretical assumption that, when an alternating current electric field is applied to a dielectric material it indicates loss and a delay to the dielectric response to the electric field described in Eq. (4), which defines the complex relative permittivity in an ac electric field. The real part of the complex permittivity (ε_r') represents the quantity of stored energy in the dielectric material from the ac field. The imaginary part (ε_r'') represents the loss to the ac electric field. Thus, the loss tangent, $\tan\delta$ is the ratio of the imaginary part to the real part of the complex relative permittivity.

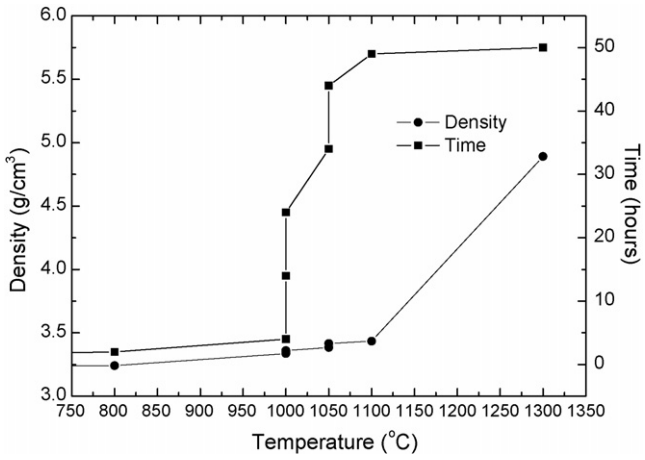

Fig. 6. Density, temperature, and time variations.

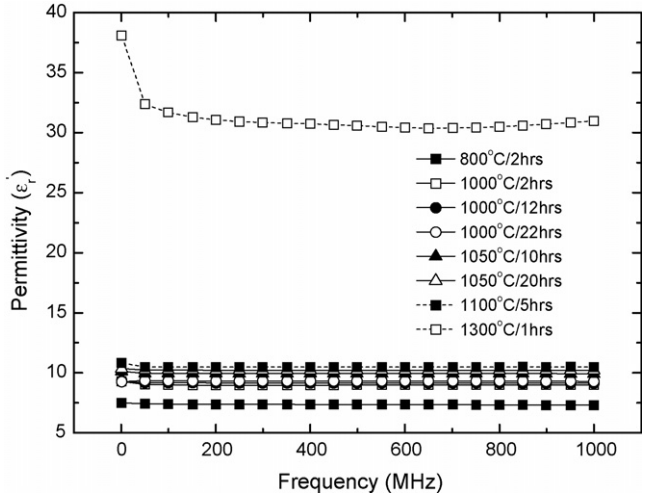

Fig. 7. Real part of relative permittivity over time, temperature, and frequency.

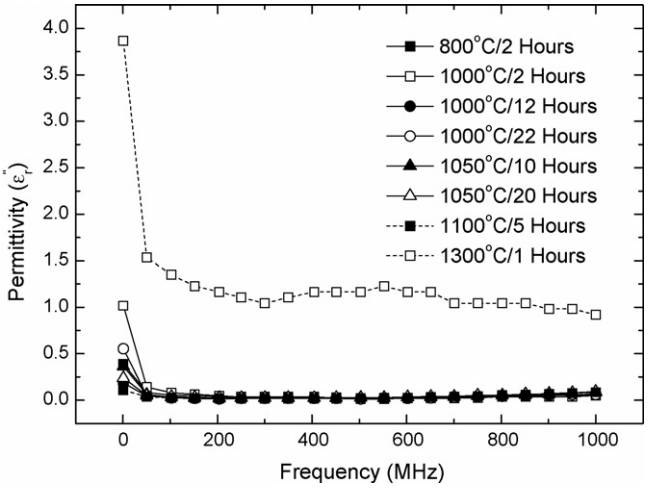

Fig. 8. Imaginary part of relative permittivity over time, frequency, and temperature.

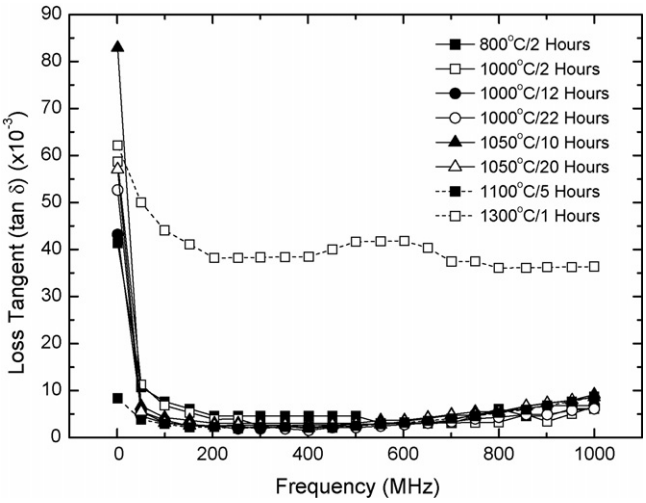

Fig. 9. Loss tangent over time, frequency and temperature.

Fig. 7 shows the real part of the complex relative permittivity (ε_r') for the samples treated isothermally. The initial value was largely constant over the frequency range and approximately equal to a value of 7. After the first sintering cycle at 800 °C for 2 h the value increased by 18% and thereafter by 1–1.5% at each additional cycle. Following a sintering cycle of 1100 °C for 5 h the ε_r' value had reached a value of 10. However, when the samples were finally sintered at 1300 °C the relative permittivity increased by nearly 200%, such that ε_r' reached a final value of 32. This value is significantly higher for a single phase and undoped BaM than those reported in the literature.[6–8] This also suggests the relative permittivity being directly proportional to the material density. Additionally, it is likely that a structural reorganization of Fe atoms is occurring whilst being coordinated variously (tetrahedral and octahedral). This would influence the electrical characteristics, i.e. channels for electron propagation. Such a final value of relative permittivity shown above would be suitable for layered patch antenna applications, for example, such as those presented by Mosallaies.[6]

The data which refers to ε_r' for the samples treated isochronally at a sintering temperature of 1000 °C are also shown in Fig. 7. The initial value of ε_r' was found to be 7.3. However, after a sintering cycle of 2 h this value increased to approximately 9.1 and to 9.3 (an increase of 27% overall) for a further sintering cycle of 10 h.

Similarly, Fig. 8 shows the imaginary component of the complex relative permittivity ε_r'' as described by Eq. (4) and is concerned with the isothermal characteristics of material properties. Again, the initial value of 0.06 was found to be largely constant over the measured frequency range. After the first sintering cycle of 800 °C for 2 h this value increased by 18%. Thereafter, at each further cycle an increase of 1–1.5% was observed until a sintering cycle of 1100 °C for 5 h where ε_r'' had now reached a value of 0.07. However, on subsequent heating these samples at the final sintering temperature of 1300 °C, ε_r'' increased by nearly 1300% to a value of 1.01. This observation mirrors the ε_r' and variation of density response as discussed earlier. This is consistent with the interpretation in terms of the influence of the structural reor-

ganisation to its final theoretical density implying less free space available within the material. This scenario is analogous to the characteristics of a suspended microstrip structure. Here, an air gap is introduced under the substrate that carries the transmission line conductor and the ground plane,[17] using suspended microstructure topology. As the air gap is increased the effective relative permittivity (ε_{eff}) is reduced. In such a case, a very small air gap causes a quite large change in ε_{eff} values simulated using equations reported in the literature by Hammerstad.[18] In the case of BaM material, the air gap refers to the amount of free space in the material and therefore is related to the density (theoretical density being zero air gap). The further the material density approaches the actual theoretical density the sharper is the increase of ε'_{r} and ε''_{r}, in agreement with the microstrip scenario. Also, the finer grain size observed in the microstructure facilitates this consequential increase in density. This marked increase in both the ε'_{r} and ε''_{r} is significant, particularly since no binder has been used in the preparative techniques. The ε''_{r} is not normally quoted as a characteristic for applications compared to ε'_r and tan δ which are more descriptive of the material electrical properties.

Fig. 8 also shows the imaginary component of the complex relative permittivity (ε''_{r}) for samples sintered isochronally at a temperature of 1000 °C. The initial value of ε''_{r} was found to be approximately 0.039. However, after a sintering cycle of 2 h this value increased to 0.046, a relatively moderate increase of 18% when compared to the samples treated at 1300 °C. A further increase of 8% to a value of 0.050 was observed following an additional treatment cycle of 10 h. On a further 10 h treatment this value reached 0.059, an additional increase of 18%. The enhancement of the dielectric variables are entirely suitable for tailored applications. Some examples may be radio absorbent material (RAM), microstrip antennas and frequency selective surfaces, etc.

A theoretical analysis of the tangent of the phase angle δ of the complex relative permittivity is defined in terms of ε'_{r} and ε''_{r} is presented below:

$$\tan\,\delta = \frac{\varepsilon''_{\text{r}}}{\varepsilon'_{\text{r}}} \tag{7}$$

$$\cos\,\delta = \frac{\varepsilon'_{\text{r}}}{|\varepsilon|} \tag{8}$$

$$\sin\,\delta = \frac{\varepsilon''_{\text{r}}}{|\varepsilon|} \tag{9}$$

From Euler's formula:

$$\varepsilon = \varepsilon'_{\text{r}} - \text{j}\varepsilon''_{\text{r}} = |\varepsilon|(\cos\,\delta - \text{j}\,\sin\,\delta) = |\varepsilon|\text{e}^{-j\delta} \tag{10}$$

If the electric field is $\mathbf{E}_{\text{o}}\cos(\omega t)$ then the electric displacement D, lags the electric field by the phase angle δ and is equal to

$$D = |\varepsilon|E_{\text{o}}\,\cos(\omega t - \delta) \tag{11}$$

Applying the theoretical description shown above, Fig. 9 thus refers to isothermally and isochronally treated samples and as such, this loss parameter follows the same trends as the ε''_{r} and ε'_{r} values.

Above 50 MHz, the initial value of tan δ for isothermally treated samples remained largely constant over the frequency range equalling to 0.0056. At 800 °C, the first sintering cycle of 2 h the value rose nominally by 2% and 1–1.5% thereafter for each further cycle. Subsequently, treatment at 1100 °C for 5 h produced a similarly low tan δ value of 0.0065. However, at an elevated final temperature of 1300 °C, the loss tangent increased by nearly 400%, such that tan δ now reached a value of 0.0329. It is unclear as to why this apparent increase in loss tangent should accompany higher sintering temperature. It is normally the case that with higher densification at elevated temperatures a reduction in loss tangent is expected. However, it is not always necessary to have low loss materials in electronic applications such as absorbers. The hexagonal ferrites are especially useful in the development of microwave absorbers, due to their large value of magnetisation, planar magnetic anisotropy, and complex permeability, which is greater than that in the microwave region.[19–21] Microwave absorption takes place due to lossy interaction between the magnetisation of ferrite material and the magnetic field of the electromagnetic wave incident on the microwave absorber.[19]

With regards to the isochronal samples at a temperature of 1000 °C the initial mean value of loss tangent over the frequency range (1 MHz–1 GHz) was found to be 0.0056. However, after a sintering cycle of 2 h this value increased to 0.0057, an increase of 2%. An additional cycle of 10 h the value rose to 0.0059, an increase of 8%. Finally after a further 10 h this value reached 0.0062, a final increase of 18%. Again, the trend of increased loss tangent values is indicated particularly when treated for higher temperatures or longer dwelling times. Hence, an optimum heat treatment protocol is necessary to maintain acceptable loss parameters where required in the application.

4. Conclusions

The paper provides high frequency dielectric characteristics of the barium hexaferrite (BaM) as a function of temperature (isothermal), time (isochronal) and frequency as well as density when prepared by co-precipitation route. It was found that a phase pure BaM can be prepared at a relatively low sintering temperature of 1050 °C. Furthermore, the high values of complex relative permittivity and low loss tangent were found to remain largely constant over the frequency range measured with a standard deviation of 0.05. The relatively flat response over frequency of the measured parameters would suggest the atomic/structural rearrangement in the BaM have not yet reached their natural resonant frequency because of their binding in the crystal. They transfer maximum energy from an electromagnetic wave in BaM at this frequency, which is known to occur no lower than 3 GHz.[6] hexagonal ferrites such as barium ferrite are the most widely used permanent magnets in the world.[22]

Acknowledgements

The authors would like to thank Mr. Martin Davies for his assistance in the Materials Preparation and Microscopy Lab-

oratory, School of Engineering, University of Warwick, and for XRD and Electron Microscopy of the dielectric materials and David Hammond for the Thermogravimetry and differential thermal analysis performed in the Department of Physics at the University of Warwick.

References

1. Pfeiffer, H., Chantrell, R. W., Görnert, P., Schüppel, W., Sinn, E. and Rösler, M., Properties of barium hexaferrite powders for magnetic recording. *Journal of Magnetics and Magnetic Material*, 1993, **125**, 373–376.
2. Smit, J. and Wijn, H. P. J., Ferrites, *Philips Technical Library*. *Eindhoven*, 1961.
3. Buchner, W., Schliebs, R., Winter, G. and Buchel, K. H., *Industrial Inorganic Chemistry*. VCH, Weinheim, 1989.
4. Sung, H. M., Chen, C. J., Ko, W. S. and Lin, H. C., Fine powder ferrite for multilayer chip inductors. *IEEE Transactions on Magnetics*, 1984, **30**, 4906–4908.
5. Zhang, H. G., Li, L. T., Ma, Z. W., Zhou, J., Yue, Z. X. and Gui, Z. L., Investigation on permeability–frequency characteristics and microstructure of composite ferrites. *Journal of Magnetism & Magnetic Material*, 2000, **218**, 67–71.
6. Mosallaei, H. and Sarabandi, K., Magneto-dielectrics in electromagnetics: concept and applications. *IEEE Transactions on Antennas & Propagation*, 2004, **52**, 1558–1567.
7. Homg, S. Y., Ho, M. C., Hsu, Y. H. and Liu, T. C., Synthesis of nanocrystalline $Ba(MnTi)_xFe_{12-2x}O_{19}$ powders by the sol–gel combustion method in a citrate acid–metal nitrates system ($x = 0,0.5,1.0,1.5,2.0$). *Journal of Magnetism & Magnetic Material*, 2004, **279**, 401–410.
8. Benito, G., Morales, M. P., Requena, J., Raposo, V., Vazquez, M. and Moya, J. S., Barium hexaferrite monodispersed nanoparticles prepared by the ceramic method. *Journal of Magnetism & Magnetic Material*, 2001, **234**, 65–72.
9. Klug, H. P. and Alexander, L. E., *X-ray Diffraction Procedures for Polycrystalline and Amorphous Materials*. Wiley, New York, 1967.
10. Shelley, B., Application Note 1217-1, "Basics of measuring the dielectric properties of materials". *Agilent Technologies*, September 2001.
11. Duval, C., *Inorganic Thermogravimetric Analysis*. Elsevier, London, 1963, pp. 533.
12. Bye, G. C. and Howard, C. R., *Journal of Applied Chemistry: Biotechnology*, 1971, **21**, 319.
13. JCPDS File Number. 27-1029, International Centre for Diffraction Data (ICDD).
14. Routil, R., Barham. *Journal of Chemistry*, 1974, **52**, 3235.
15. Townes, W. D., Fang, J. H. and Perrotta, A. J., The crystal structure and refinement of ferrimagnetic barium ferrite, $BaFe_{12}O_{19}$. *Zeitschrift fuer Kristallographie, Kristallgeometrie, Kristallphysik*, 1967, **125**, 11–23.
16. Bertaut, E. F., Deschamps, A. and Pauthenet, R., Etude de la substitution de Fe par Al, Ga et Cr dans l'hexaferrite de baryum, $BaO,(Fe_2O_3)_6$. *Comptes Rendus Hebdomadaires des Seances de l'Academie des Sciences*, 1958, **246**, 2594–2597.
17. Tomar, Bhartia, "New quasi-static models for the computer-aided design of suspended and inverted microstrip lines," *IEEE Transactions on Microwave Theory and Techniques*, vol. 35, No. 4, pp. 453–457, April 1987 [corrections No. 11, 1076 pp. November 1987].
18. Hammerstad, E. and Jensen, O., Accurate models for microstrip computer-aided design. *IEEE MTT-S Symposium Digest*, 1980, 407–409.
19. Nedkov, Karpov, A. and Petkov, V., Microwave absorption in Sc and Co–Ti substituted barium hexaferrite powder. *IEEE Transactions on Magnetics*, 1990, **26**, 1483–1484.
20. Naito, Y. and Suetake, K., Application of ferrite to electromagnetic wave absorber and its characteristics. *IEEE Transactions on Microwave Theory and Techniques*, 1971, **19**(4), 65–72.
21. Amin, M. B. and James, J. R., Techniques for the utilization of hexagonal ferrites in radar absorber. Part I. Broadband planar coating. *Radio Electron Engineers*, 1981, **51**, 209–218.
22. Hinds, G. and Coey, J. M. D., *Journal of Applied Physics*, 1998, **83**, 6447.